crystals

MDPI

Communication

Removal of Acid Orange 7 from Aqueous Solution by Metal-Organic Frameworks

Sungwon Yoon, James J. Calvo and Monica C. So *

Department of Chemistry and Biochemistry, California State University Chico, Chico, CA 95929, USA; syoon6@mail.csuchico.edu (S.Y.); jcalvo@mail.csuchico.edu (J.J.C.)

* Correspondence: mso@csuchico.edu; Tel.: +1-530-898-6554

Received: 16 November 2018; Accepted: 27 December 2018; Published: 28 December 2018



Abstract: We investigated the removal of a harmful anionic dye, acid orange 7 (AO7), from aqueous solution using metal-organic frameworks (MOFs). We prepared four different MOFs (ZIF-8, ZIF-67, UiO-66, UiO-66-NH_2) by solvothermal reactions and then tested their adsorption of AO7. Infrared spectra and adsorption capacity data confirmed the removal of AO7 from aqueous solution. The factors we investigated affecting adsorption capacity include variation of the organic linkers and metal clusters of the MOFs. Our results suggest that the hydrogen bonding, π–π interactions, and zeta potentials facilitate the removal of AO7 from water. Of the four MOFs examined, ZIF-67 exhibited the highest adsorption capacity of AO7 and can be regenerated easily.

Keywords: wastewater decontamination; metal-organic frameworks; acid orange 7; ZIF-8; ZIF-67; UiO-66; UiO-66-NH_2

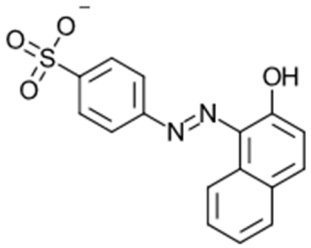
1. Introduction

Wastewater contaminated with dyes from the printing and textile industries threatens our environment and health [1–3]. Currently, two main approaches are used to remove dyes from contaminated water sources. First, chemical treatment processes, such as physical adsorption [4], electro-Fenton [5], and Fenton and Fenton-like reactions [6,7] are used to decompose refractory pollutants and improve biodegradability of dye-contaminated water, but these processes suffer from high equipment and running costs. Second, physical adsorption using granular activated carbon is popular due to its low cost and commercial availability [8–13], but it lacks synthetical or chemical tunability. Therefore, developing tunable filtration materials to remove AO7 in contaminated water becomes crucial.

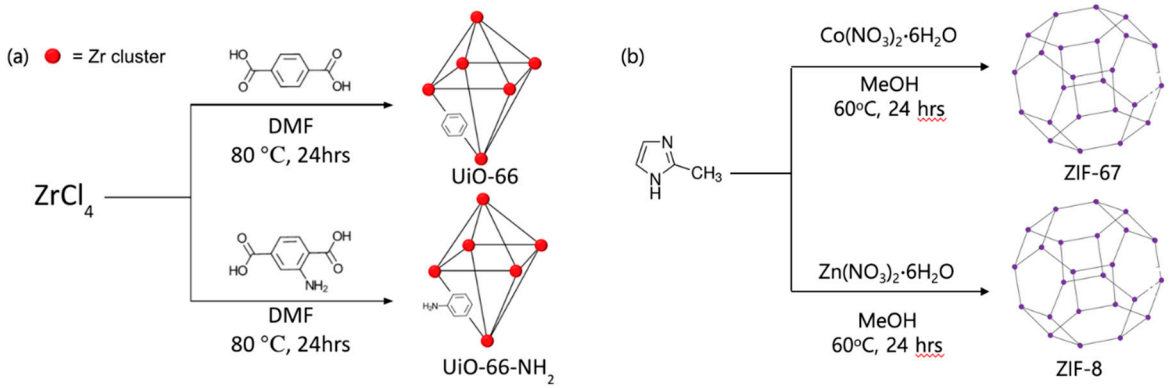
Recently, metal-organic frameworks (MOFs) have captured attention as attractive adsorbent materials, due in part to their synthetical and chemical tunability [14–16] and water stability [17–20]. These crystalline and porous materials are composed of metal ions or clusters coordinated to multitopic organic linkers. By modifying the linker, it is possible to tune the functionality, surface areas [21], and chemical stability [22,23] of the MOFs. By modifying the metal clusters, it is possible to tune the adsorption of chemical contaminants by accessing their open metal sites [24–28]. Consequently, MOFs have been implemented in a diverse array of applications, including removal of toxic materials from air and water [29,30] and adsorption, storage, and release of gases [31–35].

While previous works have investigated using MOFs for adsorptive removal of dyes, the current study differs in three important ways. First, we focus on the removal of the harmful anionic dye, acid orange 7 (AO7, Scheme 1). Others have focused on using MOFs for removal of malachite green [36], methylene blue [37], and methyl orange [38]. However, it is critical to investigate the adsorptive removal of AO7, a harmful water soluble azo-based dye resisting decomposition by biological means [39]. Due to the electron-withdrawing character of the azo group, AO7 becomes

electron deficient, reducing to carcinogenic amino compounds [40], making AO7 highly toxic and carcinogenic. If ingested, it can cause irritation to the eye, skin, mucous membrane, and upper respiratory tract [41]. Second, the present work focuses on how specifically different water-stable MOFs (Scheme 2) can be used to remove AO7. Studies involving the same MOF systems only limit their study to interactions between one MOF and one dye [36–38,42]. They do not explore the range of interactions (e.g., hydrogen bonding, π–π interactions, and zeta potentials) involved in adsorptive removal. Third, other work has investigated AO7 removal using non-MOF systems, such as activated carbon [43], soil [44], and canola stalks [45]. Even if a MOF was involved, the adsorptive mechanisms of AO7 removal were not systematically explored [42]. By exploring how hybrid porous materials like MOFs remove AO7, we can understand the factors that are important in adsorptive removal of AO7 dyes. Herein, we explore the use of MOFs as an alternative technology for the removal of AO7 from aqueous solution by exploiting hydrogen bonding, π–π stacking interactions, and zeta potentials.



Scheme 1. Chemical structure of AO7.



Scheme 2. Synthesis and simplified structure of MOFs.

2. Materials and Methods

2.1. Materials

Dimethylformamide (DMF), hydrochloric acid (HCl), zirconium(IV) chloride ($ZrCl_4$, 98%), terephthalic acid (99%), 2-aminoterephthalic acid (99%), ethanol, cobalt(II) acetate tetrahydrate ($Co(OOCCH_3)_2{\cdot}4H_2O$, 99.999%), 1,3,5-benzene tricarboxylic acid (BTC, 98%), zinc(II) acetate dihydrate ($Zn(CH_3CO_2)_2{\cdot}2H_2O$, 98%), zinc(II) nitrate hexahydrate ($Zn(NO_3)_2{\cdot}6H_2O$ 98%), 2-methylimidazole (MeIM, 99%), and methanol were purchased from Fisher Scientific (Waltham, MA, USA) and used as received.

2.2. Syntheses

2.2.1. Syntheses of UiO-66 Derivatives

UiO-66 [26]. To an 8-dram vial, 0.125 g (0.54 mmol) of $ZrCl_4$, 5 mL of DMF and 1 mL of concentrated HCl were added and sonicated about 20 min until fully dissolved. Then, 0.123 g (0.75 mmol) of terephthalic acid and 10 mL of DMF were added and sonicated for additional 20 min.

The mixture was heated at 80 °C for 24 h. The resulting solid was filtered and washed with DMF (2 × 30 mL) and ethanol (2 × 30 mL). The sample was filtered to remove residual solvents and activated at 90 °C under vacuum for 3 h. The reaction yielded 0.199 g of UiO-66.

UiO-66-NH_2 [26]. To an 8-dram vial, 0.125 g (0.54 mmol) of $ZrCl_4$, 5 mL of DMF and 1 mL of concentrated HCl were added and sonicated about 20 min until fully dissolved. Then, 0.134 g (0.75mmol) of 2-aminoterephthalic acid and 10 mL of DMF were added and sonicated for additional 20 min. The mixture was heated at 80 °C for 24 h. The resulting solid was filtered and washed with DMF (2 × 30 mL) and ethanol (2 × 30 mL). The sample was filtered to remove residual solvents and activated at 90 °C under vacuum for 3 h. The reaction yielded 0.217 g of UiO-66-NH_2.

2.2.2. Syntheses of ZIF Derivatives

ZIF-8 [46]. To a glass bottle, 4.233 g (14.2 mmol) of zinc(II) nitrate hexahydrate and 4.699 g (57.2 mmol) of 2-methylimidazole were added. To a 250 mL glass bottle, 200 mL of methanol was added. The reaction was stirred at room temperature for 1 h. The precipitate was gathered by centrifugation. and then dried under vacuum at 60 °C for 24 h. The reaction yielded 0.756 g of ZIF-8.

ZIF-67 [46]. To a glass bottle, 4.251 g (14.6 mmol) of cobalt(II) nitrate hexahydrate and 4.699 g (57.2 mmol) of 2-methylimidazole were added. To a 250 mL glass bottle, 200 mL of methanol was added. The reaction was stirred at room temperature for 1 h. The precipitate was gathered by centrifuging and then dried under vacuum at 60 °C for 24 h. The reaction yielded 0.584 g of ZIF-67.

2.2.3. Nitrogen Isotherms

UiO-66 and UiO-66-NH_2 were activated by solvent exchange to ethanol by washing. The MOF was subsequently evacuated at 80 °C under vacuum for 24 h. Since ZIF-8 and ZIF-67 were synthesized in a volatile solvent (methanol), it was sufficient to evacuate at 60 °C under vacuum for 24 h. N_2 isotherms were measured on a Quantachrome Quadrasorb pore size analyzer (Quantachrome Instruments, Boynton Beach, FL, USA) at 77 K.

2.2.4. UV-Vis Absorption Measurements

To measure MOF AO7 adsorption capacity, 100 mL samples of deionized water were contaminated with 5 mg of AO7. 10 mg of UiO-66, UiO-66-NH_2, ZIF-8, and ZIF-67 were each introduced to contaminated samples. Absorbance spectra of samples were recorded in quartz cuvettes on an Agilent UV-vis spectrophotometer (Agilent, Santa Clara, CA, USA) from 400 to 800 nm. The solutions were centrifuged before each measurement to minimize light scattering from the MOF. We recorded data hourly for a period of 6 h and then once every 24 h up to 120 h total soaking time. The decrease in light absorbance at λ_{max} of AO7 (483 nm) was used to determine the amount of AO7 adsorbed by the MOF. Beer-Lambert calculations were used to determine the concentration of AO7 which remained in the water as the absorbance at λ_{max} decreased, based on the following equation:

$$A = \varepsilon l c \tag{1}$$

where ε is the molar extinction coefficient of AO7, l is the cell length of 1 cm, and c is the concentration of the sample). The initial concentration (C_0, mg/L), and the concentration at the time of each UV-vis measurement (C_t, mg/L) were compared to determine the adsorption capacity (q_t, mg/g) at the time of each UV-vis measurement using the following equation:

$$q_t = \frac{V(C_0 - C_t)}{m} \tag{2}$$

where V is sample volume, and m is the mass of MOF in grams.

2.2.5. IR Absorption Measurements

To collect IR data, 3 mg of each MOF powder was placed into a sample port of the ThermoElectron Nicolet FTIR spectrometer (Thermo Fisher Scientific, Waltham, MA, USA). Spectra were collected from 450 to 3950 cm^{-1} with a resolution of 4 cm^{-1} with 3 scans to average.

2.2.6. Reusability Measurements

We washed the MOFs in ethanol at varying pH levels. UiO-66 and UiO-66-NH_2 in basic ethanol (pH = 9) and ZIF-8 and ZIF-67 in acidic ethanol (pH = 4). We used lower pH for ZIF-8 and ZIF-67 for washing since the lowest adsorbed amounts were at lower pH.

3. Results

We selected UiO-66, UiO-66-NH_2, ZIF-8, and ZIF-67 to perform the decontamination tests, since each are water stable and provide different factors affecting adsorption of AO7. First, by comparing UiO-66 and UiO-66-NH_2, we tested the effects of the hydrogen bonding interactions of AO7 and the zirconium metal nodes of the MOFs. Further, by comparing ZIF-8 and ZIF-67, we investigated the π–π stacking effects between the MOF organic linkers and AO7. Studies on all four MOFs investigated the significance of zeta potential on anionic dye adsorption. We performed powder x-ray diffraction (PXRD, Figures 1 and S1), scanning electron microscopy (SEM, Figure S2), infrared spectroscopy (IR, Figures 2 and 3), nitrogen (N_2) isotherms (Figure S3), UV-visible absorption spectroscopy (Figure S4), adsorption capacity experiments (Figure 4), pH dependence experiments (Table 1), and reusability experiments (Figure 5) on all MOFs.

3.1. Structural Characterization

PXRD data (Figure 1) of UiO-66, UiO-66-NH_2, ZIF-8 and ZIF-67 indicate that the MOFs were successfully synthesized. All MOFs also retained their crystallinity following adsorption of AO7. SEMs (Figure S2) further show the expected shapes of each MOF were formed.

IR data show new peaks after adsorption of AO7 in UiO-66 but not UiO-66-NH_2 (Figure 2). Since the IR spectra before and after dye adsorption are almost the same for UiO-66-NH_2 (Figure 2b), this indicates that the main functional groups are unchanged. In other words, hydrogen bonds are not formed or are very weak. Rather, there are likely coulombic interactions, so the AO7 undergoes negligible hydrogen bonding adsorption by UiO-66-NH_2. On the other hand, the IR spectra UiO-66 before and after dye adsorption (Figure 2a) show shifts in the S-O and O-H vibrations related to the formation of hydrogen bonds between the –SO_3/OH groups in AO7 and the uncoordinated –OH in UiO-66. The peaks at 1180 and and 3460 cm^{-1} related to S–O and O–H vibrations, respectively, in AO7 shift to 1140 and 3280 cm^{-1} after adsorption by UiO-66. This can also explain the higher adsorption of UiO-66 compared to UiO-66-NH_2 in Section 3.2. The proposed AO7 adsorption mechanism of UiO-66 compared to UiO-66-NH_2 is further discussed in Section 4.

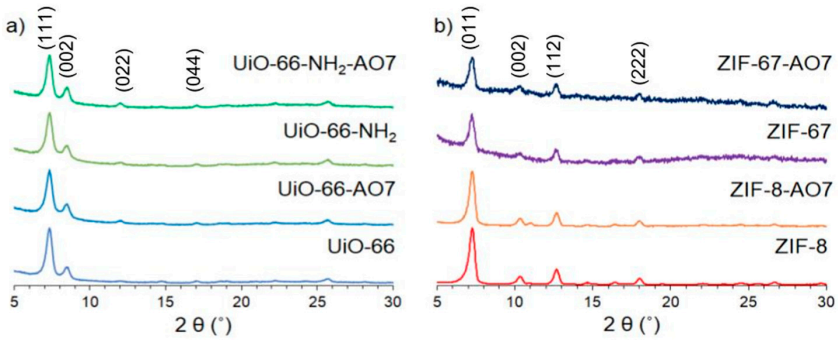


Figure 1. PXRD patterns of (**a**) UiO-66 (blue) and UiO-66-NH_2 (green) and (**b**) ZIF-8 (red) and ZIF-67 (purple) prior to and following decontamination experiments.

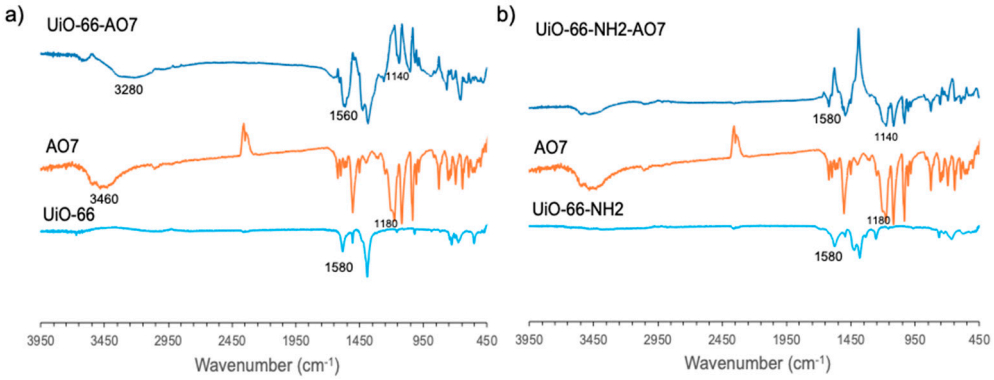


Figure 2. IR of (**a**) UiO-66 and (**b**) UiO-66-NH_2 before and after dye adsorption.

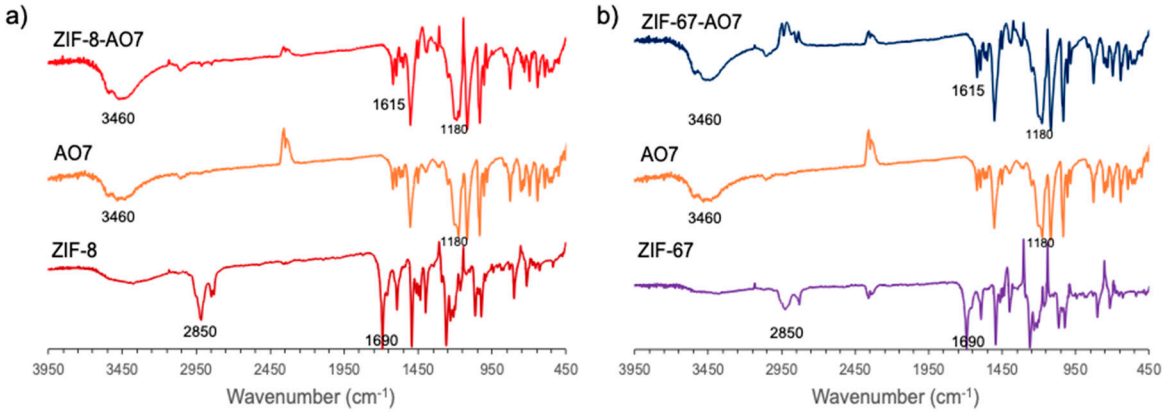


Figure 3. IR spectra of the (**a**) ZIF-8 and (**b**) ZIF-67 before and after dye adsorption.

IR measurements of ZIF-8 and ZIF-67 prior to and following decontamination experiments were also performed (Figure 3). The as-synthesized ZIF-67 and ZIF-8 exhibit peaks at 1690 and 2850 cm^{-1}, which could be attributed to the stretching modes of the C=N bonding and C-H from the aromatic ring of the 2-methylimidazole. The peak at 1615 cm^{-1} can be attributed to the C=C aromatic stretching mode. New peaks following decontamination experiments at 1180 and 3460 cm^{-1} for both MOFs correlate to sulfonate and hydroxyl stretching, respectively. They indicate surface adsorption of AO7. The proposed AO7 adsorption mechanism of ZIF-67 compared to ZIF-8 is further discussed in Section 4.

3.2. Screening of MOFs for Adsorption of AO7

Since the dimensions of AO7 are 5.44 Å × 10.03 × 15.67 Å, this suggests the pore apertures of UiO-66 (6.0 Å) and UiO-66-NH_2 (5.6 Å) can accommodate AO7 [47]. Because of the small window sizes (3.4 Å) for ZIF-8 and ZIF-67, they are not expected to adsorb AO7 as it is too large to fit inside the pores. Therefore, adsorption of ZIFs is likely to occur on their external surface [48]. Therefore, we expected the four MOFs to be appropriate for AO7 adsorption.

We initially performed small scale AO7 adsorption experiments with all four MOFs. 20 mg of each MOF were introduced to 3 mL of 0.1 μM of AO7. These experiments were monitored visually and spectrophotometrically (Figure S4). AO7 adsorption was confirmed by a visual decline in the orange color of the contaminated samples and a substantial decrease at the maximum absorbance of AO7 at 483 nm. All MOFs showed similar behavior, prompting us to scale up our investigation to explore the factors which affect AO7 adsorption. Results in Section 3.2 indicate significant variation in adsorption capacities between the MOFs.

Adsorption of AO7 by MOFs

To quantitatively investigate the MOF adsorption capacity of AO7, we introduced 10 mg of each MOF into 100 mL of water containing 5 mg of AO7. Based on the adsorption capacity data, all four MOFs had an initial increase in adsorption capacity (q_t), which then plateaued after 24 h of AO7 adsorption (Figure 4). UiO-66, UiO-66-NH_2, ZIF-8, and ZIF-67 had maximum adsorption capacities of 106.6 mg/g, 85.0 mg/g, 16.9 mg/g, and 272.7 mg/g, respectively. These experimental values have higher q_t than other MOFs and materials (Table S1). We also found that increasing the mass of MOFs will directly increase adsorption capacity.

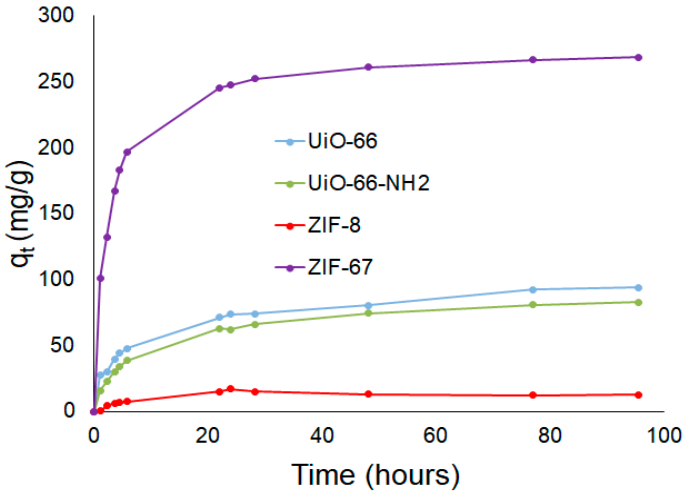


Figure 4. Adsorption capacity of AO7 in UiO-66, UiO-66-NH_2, ZIF-8, and ZIF-67 as a function of time.

Table 1 shows the changes in the adsorbed amounts of AO7 on MOFs at various pH values. The adsorption of UiO-66 and UiO-66-NH_2 of anionic dye (AO7) increases in acidic solution. This is because the surface of these MOF have free hydroxyl groups, which tend to protonate in acidic pH. Due to the electrostatic interaction with the anionic dye, sorption to the MOF occurs more easily [49,50]. Further, ZIF-67 showed increased adsorption when pH increases from pH 5.0 to 8.0 and then sharply decreases with increasing pH from 8.0 to 9.0. For ZIF-8, the adsorption of AO7 increases with increasing pH from pH 5.0–7.0 and then rapidly decreases above pH 8. There are two factors at play. First, since AO7 contains a sulfonate group, the dye exists in solution as negatively charged anions. Secondly, since the isoelectric point of the ZIF-67 is at pH of 9, it indicates that the MOF surface is positively charged when pH < 9 but negatively charged when pH > 9 [51]. The isoelectric point of ZIF-8 is at pH of 8, so the MOF surface is positively charged when pH < 7 but negatively charged when pH > 7 [52]. Therefore, at lower pH, strong electrostatic attractions occur between sulfonate groups of AO7 and the linkers of the MOFs, but excess hydrogen ions might compete with ZIF-67 or ZIF-8 in acidic solution, leading to the increase of adsorption capacity with increasing pH [53]. The highest q_t value coincides before the isoelectric points of each MOF.

Table 1. Effect of pH on adsorption of AO7 on MOFs.

pH	Adsorbed Amount (mg AO7/g Adsorbent)			
	UiO-66	**UiO-66-NH_2**	**ZIF-8**	**ZIF-67**
5	133	98	3.3	63.4
6	110	95	7.4	126.9
7	106.5	84.9	16.9	272.6
8	9.83	7.88	13.4	738
9	11.5	6.8	7.4	400

To regenerate and reuse the MOF after dye sorption, we washed the UiO-66 and UiO-66-NH_2 in basic ethanol (pH = 9) and ZIF-8 and ZIF-67 in acidic ethanol (pH = 4). We used lower pH for ZIF-8 and ZIF-67 for washing since the lowest adsorbed amounts were at lower pH, according to Table 1. As shown in Figure 5, the reusability of all MOFs up to the third cycle was stable. The adsorbed AO7 were removed efficiently from the adsorbent by simply washing with ethanol in the appropriate pH levels. This result suggests that the MOFs are suitable for adsorptive removal of the anionic dye.

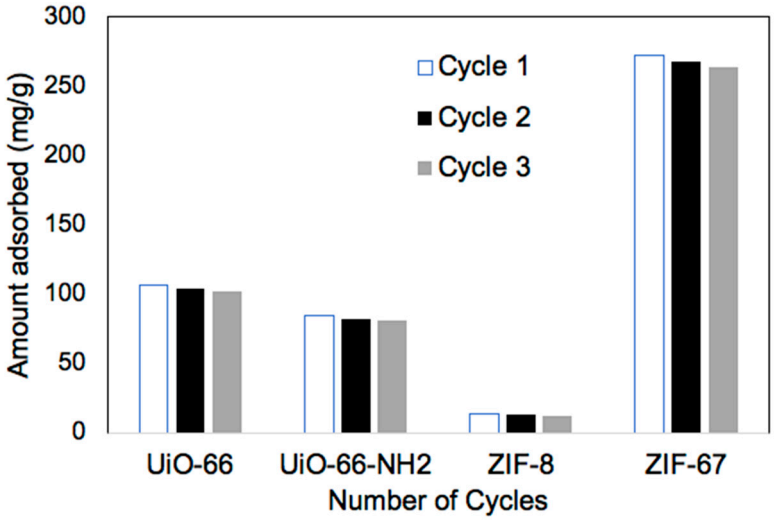


Figure 5. Reusability of MOFs for adsorption of AO7. ZIF-8 and ZIF-67 were washed with acidic ethanol (pH 4), while UiO-66 and UiO-66-NH_2 were washed with basic ethanol (pH = 9).

Furthermore, the effects of competing ions on the adsorption of AO7 were evaluated from AO7 solutions with 0.043 mol/L and 0.13 mol/L NaCl. As shown in Table S2, the q_t of AO7 decreased with increasing NaCl concentrations, suggesting that adsorption of AO7 was hindered with external ions such as Na^+ and Cl^-.

4. Discussion

Adsorptive removal of water contaminants requires understanding into the types of interactions involved between adsorbent and contaminant. The amount of AO7 adsorbed by UiO-66 and UiO-66-NH_2 increased especially at low pH with maximum adsorption capacity at pH of 5, as shown in Table 1. ZIF-8 and ZIF-67 adsorbed the most AO7 based on their isoelectric points at pH below 8 and 9, respectively.

UiO-66 and UiO-66-NH_2 demonstrated some AO7 adsorption. One reason is due to the coordination between the $Zr_6O_4(OH)_4$ nodes and oxyanions. Both monodentate and bridging motifs have been proposed [17]. A monodentate motif forms with 12-coordinated ideal nodes ($ZrO_4(OH)_4(-CO_2)_{12}$), while the bridging motif occurs with imperfect nodes ($ZrO_4(OH)_x(-CO_2)_y$). Bridging coordination between AO7 and $Zr_6O_4(OH)_4$ is likely due to the sulfonate terminus of AO7 binding to two neighboring zirconia in the metal cluster (Figure S5). Based on the monodentate model, we suspected that additional hydrogen bond donors may contribute to the adsorption of AO7 [54–59]. As evidenced by Figure 2b, very weak to no hydrogen bonding occurred between the hydroxyl of AO7 and the amine of UiO-66-NH_2. The additional amine of UiO-66-NH_2 acts as a weak base in aqueous solution, encouraging proton diffusion into the MOF. This results in positive character on the inside of UiO-66-NH_2 and a negative shift in zeta potential, compared to UiO-66. The negative surface of UiO-66-NH_2 therefore discourages anionic dye adsorption compared to UiO-66 and may result in the disparity between the maximum adsorption capacity of the two MOFs (Figure 4) [38]. Our results suggest that any potential for hydrogen bonding between the amine of UiO-66-NH_2 and AO7 may be insignificant compared to the zeta potential of the MOF.

Due to the small pore apertures of ZIF-8 and ZIF-67, the adsorption of AO7 should mainly occur at the external surface [47,54]. The adsorption capacity of ZIF-67 is sixteen times higher than in ZIF-8 (Figure 4), though both frameworks are isostructural. ZIF-8 is known to undergo surface etching after only 1 day of immersion under highly acidic environments, whereas ZIF-67 remains unaffected under various acidic pH levels [52]. Further, the imidazole ring in 2-methylimidazole has two double bonds and a pair of electrons from the protonated nitrogen, which all interact on the planar surface of the imidazole ring. Therefore, the imidazole ring can be considered as an aromatic compound which can interact with other aromatic compounds via the π–π stacking interaction with AO7 (Figure S6) [36]. Though significantly smaller than that of ZIF-67, the adsorption capacity of ZIF-8 is comparable to reported values (Table S1) [37]. This relatively low value suggests that AO7 is likely weakly interacting with the surface of ZIF-8 by π–π interactions. However, the significantly higher adsorption capacity of ZIF-67 makes it the more appealing candidate for further application as a dye adsorbent.

5. Conclusions

In summary, adsorption of aqueous AO7 by crystalline, porous, and water-stable MOFs have been explored. Of the four MOFs examined, ZIF-67 exhibited the highest adsorption capacity of AO7 and can be regenerated easily. Our findings highlight the importance of hydrogen bonding, metal node-based adsorption sites, π–π interactions, and zeta potentials, which contribute to adsorption and removal of AO7 from water. Since there is a wide spectrum of metal nodes (or clusters) and multitopic linkers potentially useful for building MOFs, a large number (while not explored herein) may potentially be attractive candidates for adsorption of AO7. These MOF candidates must have high adsorption capacity, water stability, and facile regeneration to maximize adsorption of other harmful dyes in wastewater. The future of exploiting the chemical and synthetic tunability of MOFs for water decontamination is indeed extremely promising.

Supplementary Materials: The following are available online at http://www.mdpi.com/2073-4352/9/1/17/s1, Figure S1. Full spectrum of PXRD of a) UiO-66 and UiO-66-NH_2 and b) ZIF-8 and ZIF-67 before and after dye Adsorption, Figure S2. SEM image of expected sodalite structures of (a) ZIF-8 and (b) ZIF-67 and octahedral shapes of (c) UiO-66-NH_2, and (d) UiO-66, Figure S3. N_2 isotherms and BET surface areas of (a) UiO-66 (blue) and UiO-66-NH_2 (green) and (b) ZIF-8 (red) and ZIF-67 (purple) before and after AO7 adsorption, Figure S4. UV-visible absorbance spectra of water samples containing AO7 dye with (a) UiO-66, (b) UiO-66-NH_2, (c) ZIF-8, and (d) ZIF-67. These were recorded over the course of the decontamination experiment, Figure S5. Proposed interaction between AO7 and UiO-66 through monodentate and bridging motifs. Black lines represents a coordinating carboxylate from the organic linkers, Figure S6. Proposed mechanism of ZIF-8 and ZIF-67 and AO7 interaction. Black lines represent methylimidazole linkers and purple dots represent metal ions. Dashed lines indicate proposed pi-pi stacking interactions, Table S1. Comparison of the maximum adsorption abilities of different MOFs for the removal of dyes, Table S2. Effect of chloride anions on adsorption of AO7 by studied MOFs.

Author Contributions: Conceptualization, M.C.S.; Methodology, S.Y. and J.J.C.; Formal Analysis, M.C.S., S.Y. and J.J.C.; Investigation, M.C.S., S.Y. and J.J.C.; Resources, M.C.S., S.Y. and J.J.C.; Writing—Original Draft Preparation, M.C.S., J.J.C. and S.Y.; Writing—Review & Editing, M.C.S., J.J.C. and S.Y.; Supervision, M.C.S.; Project Administration, M.C.S.; Funding Acquisition, M.C.S.

Funding: This project was funded through Chico STEM Connections Collaborative (CSC^2), California State University Program for Education & Research in Biotechnology (CSUPERB), and CSU Council on Ocean Affairs, Science & Technology (CSU COAST).

Acknowledgments: The authors would like to acknowledge useful discussion with David Ball (CSU Chico) and the use of Quantachrome Quadrasorb pore size analyzer at Sandia National Laboratories (Livermore, CA).

Conflicts of Interest: The authors declare no conflict of interest.

References

1. Banat, I.M.; Nigam, P.; Singh, D.; Marchant, R. Microbial Decolorization of Textile-Dye-Containing Effluents: A Review. *Bioresour. Technol.* **1996**, *58*, 217–227. [CrossRef]
2. Clarke, E.A.; Anliker, R. Organic Dyes and Pigments. In *Handbook of Environmental Chemistry*; Springer: New York, NY, USA, 1980.

3. Wang, J.; Huang, C.P.; Allen, H.E.; Cha, D.K.; Kim, D.W. Adsorption Characteristics of Dye onto Sludge Particulates. *J. Colloid Interface Sci.* **1998**, *208*, 518–528. [CrossRef] [PubMed]
4. Ahmad, A.A.; Hameed, B.H. Effect of preparation conditions of activated carbon from bamboo waste for real textile wastewater. *J. Hazard. Mater.* **2010**, *173*, 487–493. [CrossRef] [PubMed]
5. Ruiz, E.J.; Arias, C.; Brillas, E.; Hernández-Ramírez, A.; Peralta-Hernández, J.M. Mineralization of Acid Yellow 36 azo dye by electro-Fenton and solar photoelectro-Fenton processes with a boron-doped diamond anode. *Chemosphere* **2011**, *82*, 495–501. [CrossRef] [PubMed]
6. Kang, S.F.; Liao, C.H.; Po, S.T. Decolorization of textile wastewater by photo-fenton oxidation technology. *Chemosphere* **2000**, *41*, 1287–1294. [CrossRef]
7. Kang, S.F.; Liao, C.H.; Chen, M.C. Pre-oxidation and coagulation of textile wastewater by the Fenton process. *Chemosphere* **2002**, *46*, 923–928. [CrossRef]
8. Malik, P.K. Dye removal from wastewater using activated carbon developed from sawdust: Adsorption equilibrium and kinetics. *J. Hazard. Mater.* **2004**, *113*, 81–88. [CrossRef]
9. Crini, G.; Peindy, H.N.; Gimbert, F.; Robert, C. Removal of C.I. Basic Green 4 (Malachite Green) from aqueous solutions by adsorption using cyclodextrin-based adsorbent: Kinetic and equilibrium studies. *Sep. Purif. Technol.* **2007**, *53*, 97–110. [CrossRef]
10. Malik, R.; Ramteke, D.S.; Wate, S.R. Adsorption of malachite green on groundnut shell waste based powdered activated carbon. *Waste Manag.* **2007**, *27*, 1129–1138. [CrossRef]
11. Hameed, B.H.; El-Khaiary, M.I. Equilibrium, kinetics and mechanism of malachite green adsorption on activated carbon prepared from bamboo by K_2CO_3 activation and subsequent gasification with CO_2. *J. Hazard. Mater.* **2008**, *157*, 344–351. [CrossRef]
12. Bello, O.S.; Ahmad, M.A. Coconut (Cocos nucifera) shell based activated carbon for the removal of malachite green dye from aqueous solutions. *Sep. Sci. Technol.* **2011**, *47*, 903–912. [CrossRef]
13. Derylo-Marczewska, A. Analysis of the adsorption equilibrium for the system dilute aqueous solution of dissociating organic substance-activated carbon. *Langmuir* **1993**, *9*, 2344–2350. [CrossRef]
14. Audu, C.O.; Nguyen, H.G.T.; Chang, C.Y.; Katz, M.J.; Mao, L.; Farha, O.K.; Hupp, J.T.; Nguyen, S.T. The dual capture of As V and As III by UiO-66 and analogues. *Chem. Sci.* **2016**, *7*, 6492–6498. [CrossRef] [PubMed]
15. Howarth, A.J.; Katz, M.J.; Wang, T.C.; Platero-Prats, A.E.; Chapman, K.W.; Hupp, J.T.; Farha, O.K. High efficiency adsorption and removal of selenate and selenite from water using metal-organic frameworks. *J. Am. Chem. Soc.* **2015**, *137*, 7488–7494. [CrossRef] [PubMed]
16. Park, K.S.; Ni, Z.; Côté, A.P.; Choi, J.Y.; Huang, R.; Uribe-Romo, F.J.; Chae, H.K.; O'Keeffe, M.; Yaghi, O.M. Exceptional chemical and thermal stability of zeolitic imidazolate frameworks. *Proc. Natl. Acad. Sci. USA* **2006**, *103*, 10186–10191. [CrossRef] [PubMed]
17. DeCoste, J.B.; Peterson, G.W.; Jasuja, H.; Glover, T.G.; Huang, Y.-G.; Walton, K.S. Stability and degradation mechanisms of metal-organic frameworks containing the $Zr_6O_4(OH)_4$ secondary building unit. *J. Mater. Chem. A* **2013**, *1*, 5642. [CrossRef]
18. Kandiah, M.; Nilsen, M.H.; Usseglio, S.; Jakobsen, S.; Olsbye, U.; Tilset, M.; Larabi, C.; Quadrelli, E.A.; Bonino, F.; Lillerud, K.P. Synthesis and Stability of Tagged UiO-66 Zr-MOFs. *Chem. Mater.* **2010**, *22*, 6632–6640. [CrossRef]
19. Mondloch, J.E.; Katz, M.J.; Planas, N.; Semrouni, D.; Gagliardi, L.; Hupp, J.T.; Farha, O.K. Are Zr_6-based MOFs water stable? Linker hydrolysis vs. capillary-force-driven channel collapse. *Chem. Commun.* **2014**, *50*, 8944–8946. [CrossRef]
20. Jiang, J.-Q.; Yang, C.-X.; Yan, X.-P. Zeolitic imidazolate framework-8 for fast adsorption and removal of benzotriazoles from aqueous solution. *ACS Appl. Mater. Interfaces* **2013**, *5*, 9837–9842. [CrossRef]
21. Farha, O.K.; Eryazici, I.; Jeong, N.C.; Hauser, B.G.; Wilmer, C.E.; Sarjeant, A.A.; Snurr, R.Q.; Nguyen, S.T.; Yazaydın, A.Ö.; Hupp, J.T. Metal-Organic Framework Materials with Ultrahigh Surface Areas: Is the Sky the Limit? *J. Am. Chem. Soc.* **2012**, *134*, 15016–15021. [CrossRef]
22. Gutov, O.V.; Bury, W.; Gomez-Gualdron, D.A.; Krungleviciute, V.; Fairen-Jimenez, D.; Mondloch, J.E.; Sarjeant, A.A.; Al-Juaid, S.S.; Snurr, R.Q.; Hupp, J.T.; et al. Water-Stable Zirconium-Based Metal-Organic Framework Material with High-Surface Area and Gas-Storage Capacities. *Chem. Eur. J.* **2014**, *20*, 12389–12393. [CrossRef] [PubMed]

23. Wang, T.C.; Bury, W.; Gómez-Gualdrón, D.A.; Vermeulen, N.A.; Mondloch, J.E.; Deria, P.; Zhang, K.; Moghadam, P.Z.; Sarjeant, A.A.; Snurr, R.Q.; et al. Ultrahigh Surface Area Zirconium MOFs and Insights into the Applicability of the BET Theory. *J. Am. Chem. Soc.* **2015**, *137*, 3585–3591. [CrossRef] [PubMed]
24. Cavka, J.H.; Jakobsen, S.; Olsbye, U.; Guillou, N.; Lamberti, C.; Bordiga, S.; Lillerud, K.P. A new zirconium inorganic building brick forming metal organic frameworks with exceptional stability. *J. Am. Chem. Soc.* **2008**, *130*, 13850–13851. [CrossRef] [PubMed]
25. Valenzano, L.; Civalleri, B.; Chavan, S.; Bordiga, S.; Nilsen, M.H.; Jakobsen, S.; Lillerud, K.P.; Lamberti, C. Disclosing the complex structure of UiO-66 metal organic framework: A synergic combination of experiment and theory. *Chem. Mater.* **2011**, *23*, 1700–1718. [CrossRef]
26. Katz, M.J.; Brown, Z.J.; Colón, Y.J.; Siu, P.W.; Scheidt, K.A.; Snurr, R.Q.; Hupp, J.T.; Farha, O.K. A facile synthesis of UiO-66, UiO-67 and their derivatives. *Chem. Commun.* **2013**, *49*, 9449–9451. [CrossRef] [PubMed]
27. Furukawa, H.; Gándara, F.; Zhang, Y.B.; Jiang, J.; Queen, W.L.; Hudson, M.R.; Yaghi, O.M. Water adsorption in porous metal–organic frameworks and related materials. *J. Am. Chem. Soc.* **2014**, *136*, 4369–4381. [CrossRef] [PubMed]
28. Wu, H.; Chua, Y.S.; Krungleviciute, V.; Tyagi, M.; Chen, P.; Yildirim, T.; Zhou, W. Unusual and Highly Tunable Missing-Linker Defects in Zirconium Metal-Organic Framework UiO-66 and Their Important Effects on Gas Adsorption. *J. Am. Chem. Soc.* **2013**, *135*, 10525–10532. [CrossRef] [PubMed]
29. Barea, E.; Montoro, C.; Navarro, J.A.R. Toxic gas removal-Metal-organic frameworks for the capture and degradation of toxic gases and vapours. *Chem. Soc. Rev.* **2014**, *43*, 5419–5430. [CrossRef]
30. DeCoste, J.B.; Peterson, G.W. Metal-Organic Frameworks for Air Purification of Toxic Chemicals. *Chem. Rev.* **2014**, *114*, 5695–5727. [CrossRef]
31. Zhang, K.D.; Tsai, F.C.; Ma, N.; Xia, Y.; Liu, H.L.; Zhan, X.Q.; Yu, X.Y.; Zeng, X.Z.; Jiang, T.; Shi, D.; et al. Adsorption behavior of high stable Zr-based MOFs for the removal of acid organic dye from water. *Materials* **2017**, *10*, 205. [CrossRef]
32. Khan, N.A.; Hasan, Z.; Jhung, S.H. Adsorptive removal of hazardous materials using metal-organic frameworks (MOFs): A review. *J. Hazard. Mater.* **2013**, *244–245*, 444–456. [CrossRef] [PubMed]
33. Dincă, M.; Long, J.R. Hydrogen Storage in Microporous Metal–Organic Frameworks with Exposed Metal Sites. *Angew. Chem. Int. Ed.* **2008**, *47*, 6766–6779. [CrossRef] [PubMed]
34. Li, J.-R.; Kuppler, R.J.; Zhou, H.-C. Selective gas adsorption and separation in metal-organic frameworks. *Chem. Soc. Rev.* **2009**, *38*, 1477–1504. [CrossRef] [PubMed]
35. Farha, O.K.; Yazaydın, A.Ö.; Eryazici, I.; Malliakas, C.D.; Hauser, B.G.; Kanatzidis, M.G.; Nguyen, S.T.; Snurr, R.Q.; Hupp, J.T. De novo synthesis of a metal-organic framework material featuring ultrahigh surface area and gas storage capacities. *Nat. Chem.* **2010**, *2*, 944–948. [CrossRef] [PubMed]
36. Lin, K.Y.A.; Chang, H.A. Ultra-high adsorption capacity of zeolitic imidazole framework-67 (ZIF-67) for removal of malachite green from water. *Chemosphere* **2015**, *139*, 624–631. [CrossRef] [PubMed]
37. Zheng, J.; Cheng, C.; Fang, W.J.; Chen, C.; Yan, R.W.; Huai, H.X.; Wang, C.C. Surfactant-free synthesis of a Fe_3O_4@ZIF-8 core–shell heterostructure for adsorption of methylene blue. *CrystEngComm* **2014**, *16*, 3960–3964. [CrossRef]
38. Chen, Q.; He, Q.; Lv, M.; Xu, Y.; Yang, H.; Liu, X. Selective adsorption of cationic dyes by UiO-66-NH_2. *Appl. Surf. Sci.* **2015**, *327*, 77–85. [CrossRef]
39. Anliker, R. Organic Colorants Interpretation of Mammalian-, Geno- and Ecotoxicity Data in Terms of Potential Risk. In *Toxic Hazard Assessment of Chemicals*; Richardson, M., Ed.; The Royal Society of Chemistry: London, UK, 1986; pp. 166–187.
40. Knackmuss, H.J. Basic Knowledge and Perspectives of Bioelimination of Xenobiotic Compounds. *J. Biotechnol.* **1996**, *51*, 287. [CrossRef]
41. Cartwright, R.A. Historical and Modern Epidemiological Studies on Populations Exposed to N-substituted Aryl Compounds. *Environ. Health Perspect.* **1983**, *49*, 13–19. [CrossRef]
42. Tsai, F.C.; Xia, Y.; Ma, N.; Shi, J.J.; Jiang, T.; Chiang, T.C.; Zhang, Z.C.; Tsen, W.C. Adsorptive removal of acid orange 7 from aqueous solution with metal-organic framework material, iron (III) trimesate. *Desalin. Water Treat.* **2016**, *57*, 3218–3226. [CrossRef]
43. Samarghandi, M.R.; Poormohammadi, A.; Fatemeh, N.; Ahmadian, M. Removal of acid orange 7 from aqueous solution using activated carbon and graphene as adsorbents. *Fresenius Environ. Bull.* **2015**, *24*, 1841–1851.

44. Smaranda, C.; Bulgariu, D.; Gavrilescu, M. An investigation of the sorption of acid orange 7 from aqueous solution onto soil. *Environ. Eng. Manag. J.* **2009**, *8*, 1391–1402. [CrossRef]
45. Hamzeh, Y.; Izadyar, S.; Azadeh, E.; Abyaz, A.; Asadollahi, Y. Application of Canola Stalks Waste as Adsorbent of Acid Orange 7 from Aqueous Solution. *Iran. J. Health Environ.* **2011**, *4*, 49–56.
46. Sun, W.; Zhai, X.; Zhao, L. Synthesis of ZIF-8 and ZIF-67 nanocrystals with well-controllable size distribution through reverse microemulsions. *Chem. Eng. J.* **2016**, *289*, 59–64. [CrossRef]
47. Zhao, X.; Bu, X.; Wu, T.; Zheng, S.-T.; Wang, L.; Feng, P. Selective anion exchange with nanogated isoreticular positive metal-organic frameworks. *Nat. Commun.* **2013**, *4*, 2344. [CrossRef] [PubMed]
48. Kang, X.-Z.; Song, Z.-W.; Shi, Q.; Dong, J.-X. Utilization of zeolite imidazolate framework as an adsorbent for the removal of dye from aqueous solution. *Asian J. Chem.* **2013**, *25*, 8324–8328. [CrossRef]
49. Vlasova, E.A.; Shalunova, N.K.; Makarova, A.S.; Kudrik, E.V.; Makarov, S.V. Metal-Organic Frameworks Based on Terephthalic Acid: Sorbents of Organic Dyes. *Russ. J. Appl. Chem.* **2014**, *87*, 1065–1069. [CrossRef]
50. Lin, K.Y.A.; Liu, Y.T.; Chen, S.Y. Adsorption of fluoride to UiO-66-NH_2 in water: Stability, kinetic, isotherm and thermodynamic studies. Journal of colloid and interface science. *J. Colloid Interface Sci.* **2016**, *461*, 79–87. [CrossRef]
51. Du, X.; Wang, C.; Liu, J.; Zhao, X.; Zhong, J.; Li, Y.; Li, J.; Wang, P. Extensive and selective adsorption of ZIF-67 towards organic dyes: Performance and mechanism. *J. Colloid Interface Sci.* **2017**, *506*, 437–441. [CrossRef]
52. Jung, BK.; Jun, JW.; Hasan, Z.; Jhung, SH. Adsorptive removal of p-arsanilic acid from water using mesoporous zeolitic imidazolate framework-8. *Chem. Eng. J.* **2015**, *267*, 9–15. [CrossRef]
53. Lin, K.Y.A.; Chang, H. Zeolitic Imidazole Framework-67 (ZIF-67) as a heterogeneous catalyst to activate peroxymonosulfate for degradation of Rhodamine B in water. *J. Taiwan Inst. Chem. Eng.* **2015**, *53*, 40–45. [CrossRef]
54. Li, Y.; Zhou, K.; He, M.; Yao, J. Synthesis of ZIF-8 and ZIF-67 using mixed base and their dye adsorption. *Micropor. Mesopor. Mater.* **2016**, *234*, 287–292. [CrossRef]
55. Hasan, Z.; Tong, M.; Jung, B.K.; Ahmed, I.; Zhong, C.; Jhung, S.H. Adsorption of pyridine over amino-functionalized metal-organic frameworks: Attraction via hydrogen bonding versus base–base repulsion. *J. Phys. Chem. C* **2014**, *118*, 21049–21056. [CrossRef]
56. Zhao, X.; Wang, K.; Gao, Z.; Gao, H.; Xie, Z.; Du, X.; Huang, H. Reversing the dye adsorption and separation performance of metal-organic frameworks via introduction of –SO_3H groups. *Ind. Eng. Chem. Res.* **2017**, *56*, 4496–4501. [CrossRef]
57. Wang, M.M.; Wei, Z.; Xu, L.; Liu, B.; Jiao, H. Two Temperature-Controlled Zinc Coordination Polymers: Ionothermal Synthesis, Properties, and Dye Adsorption. *Eur. J. Inorg. Chem.* **2018**, *7*, 932–939. [CrossRef]
58. Hahm, H.; Kim, S.; Ha, H.; Jung, S.; Kim, Y.; Yoon, M.; Kim, M. Charged functional group effects on a metal-organic framework for selective organic dye adsorptions. *Cryst. Eng. Commun.* **2015**, *17*, 8418–8422. [CrossRef]
59. Kumar, S.; Verma, G.; Gao, W.Y.; Niu, Z.; Wojtas, L.; Ma, S. Anionic Metal-Organic Framework for Selective Dye Removal and CO_2 Fixation. *Eur. J. Inorg. Chem.* **2016**, *27*, 4373–4377. [CrossRef]



© 2018 by the authors. Licensee MDPI, Basel, Switzerland. This article is an open access article distributed under the terms and conditions of the Creative Commons Attribution (CC BY) license (http://creativecommons.org/licenses/by/4.0/).